electronics

MDPI

Article

Geometry Optimization of Stratospheric Pseudolite Network for Navigation Applications

Yi Qu [1,2,*], Sheng Wang [1,2], Hui Feng [1] and Qiang Liu [1]

[1] Aerospace Information Research Institute, Chinese Academy of Sciences, Beijing 100094, China; wangsheng@aircas.ac.cn (S.W.); fenghui@aircas.ac.cn (H.F.); liuqiang@aircas.ac.cn (Q.L.)
[2] University of Chinese Academy of Sciences, Beijing 100049, China
* Correspondence: quyi@aircas.ac.cn

Abstract: A stratospheric pseudolite (SP) is a pseudolite installed on a stratospheric airship. A stratospheric pseudolite network (SPN) is composed of multiple SPs, which shows promising potential in navigation applications because of its station-keeping capability, long service duration, and flexible deployment. Most traditional research about SPN geometry optimization has centered on geometric dilution of precision (GDOP). However, previous research rarely dealt with the topic of how SPN geometry configuration not only affects its GDOP, but also affects its energy balance. To obtain an optimal integrated performance, this paper employs the proportion of energy consumption in energy production as an indicator to assess SPN energy status and designs a composite indicator including GDOP and energy status to assess SPN geometry performance. Then, this paper proposes an SPN geometry optimization algorithm based on gray wolf optimization. Furthermore, this paper implements a series of simulations with an SPN composed of six SPs in a specific service area. Simulations show that the proposed algorithm can obtain SPN geometry solutions with good GDOP and energy balance performance. Also, simulations show that in the supposed scenarios and the specific area, a higher SP altitude can improve both GDOP and energy balance, while a lower SP latitude can improve SPN energy status.

Keywords: stratospheric airship; pseudolite network; geometric dilution of precision (GDOP); energy balance; gray wolf optimization

Citation: Qu, Y.; Wang, S.; Feng, H.; Liu, Q. Geometry Optimization of Stratospheric Pseudolite Network for Navigation Applications. *Electronics* **2024**, *13*, 2397. https://doi.org/10.3390/electronics13122397

Academic Editor: Paul Mitchell

Received: 12 April 2024
Revised: 4 June 2024
Accepted: 5 June 2024
Published: 19 June 2024

1. Introduction

Stratospheric airships are flight vehicles that can keep their flight altitude by buoyance. They can reside in the lower portion of the stratosphere and perform station-keeping missions for a long time. This capability can provide a very efficient flight for many missions, such as science exploration, communications, earth observations, and navigations.

Researchers have proposed the concept of stratospheric pseudolites (SPs), which means to install transmitters on stratospheric airships to send out GPS-like signals to improve GNSS performance. Furthermore, a stratospheric pseudolite network (SPN) can be constructed by multiple SPs, which can provide independent positioning, GNSS augmentation and other services, especially in case of degraded visibility of GNSS signals. An SPN can provide many advantages such as wide coverage, long service duration, and flexible deployment; therefore, it has attracted abundant attention. Tsujii established a minimum configuration of a GPS/SP system to augment GPS and implemented experiments in both static and kinematic modes [1]. Dovis introduced an SPN system architecture, and discussed some key issues about SPN performance, including SP positioning, pseudo-ephemeris broadcasting, and GDOP improvement [2]. Zheng carried out simulations for SPN in urban areas and proved its effect on improving the horizontal dilution of precision (HDOP) and 3D positioning accuracy [3]. Chandu designed an SPN framework, described

its dataflow and mathematical model, and compared the feasibility of various SPN geometry configurations [4]. Dai presented SPN modeling strategies to deal with positioning error sources and proposed geometry optimization solutions for two application scenarios [5].

In previous research about SPN, geometry configuration has been identified as a critical factor affecting its positioning performance significantly. A series of approaches have been discussed to optimize the SPN geometry configuration, which can be divided into empirical methods and meta-heuristic optimization methods.

With empirical methods, Fateev suggested that an ideal pseudolite network should be composed of 5–10 pseudolites, which should be distributed along the edge of the service area and at different altitudes [6]. Sang studied the relationship between network geometry layout and geometric dilution of precision (GDOP) and illustrated three defective layouts that should be avoided in practice [7]. Hu, Gao, and Yang provided different geometry configurations for four SPs, five SPs, and six SPs, respectively, to minimize GDOP based on priori theories [8–10].

As to meta-heuristic optimization methods, Mosavi presented a pseudolite network geometry design approach with multiple evolutionary algorithms, including the genetic algorithm (GA), simulated annealing algorithm (SA), and particle swarm optimization algorithm (PSO) [11]. Shao offered a design strategy for pseudolite network geometry based on PSO and carried out indoor tests [12]. Tang put forward a multi-objective PSO algorithm for pseudolite network geometry design, whose purpose was to maximize the visual area while minimizing GDOP [13]. Yang adopted GA to search for optimal SPN to reduce the ephemeris error, ranging error, and positioning error in GNSS augmentation [14]. Chen utilized improved GA to select the best configuration aiming at enhancing accuracy in mobile positioning [15]. Song proposed an adaptive GA to realize geometry optimization under multiple constraints, especially under orographic terrain constraints and traffic facility constraints [16].

The studies listed above provided rich references for SPN geometry design. However, the energy balance requirement of SPN has rarely been analyzed, with even less consideration of the integrated optimization of SPN energy balance and GDOP.

In fact, the energy system of an SP is quite different from that of other aerial vehicles because it is always in the dynamic variation of energy production and energy consumption in its service duration. The balance between energy production and energy consumption is very vulnerable, since the energy gained from the solar arrays is quite limited, while the energy consumption due to resisting wind is enormous. Once its energy consumption exceeds energy production, an SP will encounter difficulties sustaining normal operation, making its service availability and continuity degrade greatly.

The main problem is that GDOP, SP energy production, and SP energy consumption are all governed by the SPN configuration. If GDOP is regarded as the sole objective during the course of SPN geometry design, an SPN unable to keep energy balance may be obtained. To avoid such an unpractical result, this paper proposes an SPN geometry design algorithm based on gray wolf optimization (GWO), pursuing the integrated optimization of GDOP and SPN energy balance.

This paper assumes the transmitting antennas onboard are directional antennas pointing down to the ground. Furthermore, this paper makes the following assumptions for an SP in its service duration, as Table 1 illustrates:

Table 1. Assumptions for an SP in its service duration.

Symbolic	Physical Meaning	Assumption
λ_j	longitude of the j-th SP	remain constant
Φ_j	latitude of the j-th SP	remain constant
h_j	altitude of the j-th SP	remain constant, 18–20 km as the preferred interval, and 20–28 km as the alternative interval [17,18]

Table 1. *Cont.*

Symbolic	Physical Meaning	Assumption
γ_j	yaw angle of the j-th SP	remain constant, do not affect the vector between a user receiver to the SP
α_j	pitch angle of the j-th SP	0
β_j	roll angle of the j-th SP	0
m_j	mass of the j-th SP	remain constant
J_{kaj}	energy spent on keeping flight altitude of the j-th SP	0
η_{vj}	photoelectric conversion efficiency	remain constant
J_{loss}	energy loss in the process of transfer, charging, storage, and discharging	0

The rest of this paper is organized as follows. The GDOP of SPN is analyzed in Section 2, an energy balance model of SPN is established in Section 3, an SPN geometry design algorithm based on GWO is proposed in Section 4, simulations and discussions are presented in Section 5, and conclusions and future works finally complete this paper.

2. GDOP of an SPN

GDOP is a widely used indicator in SPN performance assessment. It is defined as the statistics ratio of positioning accuracy, timing accuracy, and ranging accuracy. Given the same pseudo-range error, the smaller the GDOP is, the smaller the positioning error and timing error are.

In this paper, the GDOP of an SPN is defined as the average GDOP of multiple users in the SPN service area, which can be described by Equation (1).

$$GDOP_N = \frac{1}{n_u}\sum_{i=1}^{n_u} GDOP_i \tag{1}$$

In Equation (1), n_u represents the number of observers distributed in the service area. $GDOP_i$ represents the GDOP of the i-th user, which can be calculated by Equations (2)–(4) [19–21].

$$GDOP_i = \sqrt{tr(\boldsymbol{H}_i^T \boldsymbol{H}_i)^{-1}} \tag{2}$$

$$\boldsymbol{H}_i = \begin{bmatrix} a_{xi1} & a_{yi1} & a_{zi1} & 1 \\ a_{xi2} & a_{yi2} & a_{zi2} & 1 \\ \vdots & \vdots & \vdots & \vdots \\ a_{xin_p} & a_{yin_p} & a_{zin_p} & 1 \end{bmatrix} \tag{3}$$

$$\begin{aligned} a_{xij} &= \frac{x_j - x_{ui}}{\sqrt{(x_j - x_{ui})^2 + (y_j - y_{ui})^2 + (z_j - z_{ui})^2}} \\ a_{yij} &= \frac{y_j - y_{ui}}{\sqrt{(x_j - x_{ui})^2 + (y_j - y_{ui})^2 + (z_j - z_{ui})^2}} \\ a_{zij} &= \frac{z_j - z_{ui}}{\sqrt{(x_j - x_{ui})^2 + (y_j - y_{ui})^2 + (z_j - z_{ui})^2}} \end{aligned} \tag{4}$$

In Equations (2)–(4), $\boldsymbol{H_i}$ represents the observation matrix of the i-th user, n_p represents the number of SPs in the network, a_{xij}, a_{yij}, a_{zij} represent the vector components between the i-th user receiver and the j-th SP, (x_{ui}, y_{ui}, z_{ui}) represent the position of the i-th user in the ECEF (Earth-Centered, Earth-Fixed) coordinate system, and (x_j, y_j, z_j) represent the position of the j-th SP in the ECEF coordinate system, which is gained from (λ_j, Φ_j, h_j) by coordinate transformation.

3. Energy Balance of an SPN

3.1. Energy Consumption of an SP

SP energy is used to support its equipment, such as the propeller, flight controller, TT&C (Telemetry, Tracking, and Command) system, and mission payloads. The propeller consumes a great deal of energy, and it is deeply affected by SP position and attitude. The energy consumption of the other equipment is slightly affected by SP position and attitude, and their requested power is assumed to be constant in this paper.

3.1.1. Energy Consumption of a Propeller

For the j-th SP, the power required by its propeller can be estimated by Equation (5) [22].

$$P_{ej} = \boldsymbol{T}_j \boldsymbol{U}_j / \eta_{pj} / \eta_{ej} \tag{5}$$

In Equation (5):
P_{ej} represents propeller power;
$\boldsymbol{T}_j$ represents thrust generated by the propeller;
$\boldsymbol{U}_j$ represents airspeed;
η_{pj} and η_{ej} represent propeller efficiency and motor efficiency, respectively, which can be assumed as constants according to the analysis in [22].

So, the energy consumption of the propulsion propeller of the j-th SP, represented by J_{ej}, can be expressed by Equation (6).

$$J_{ej} = \int_0^{t_s} \boldsymbol{T}_j \boldsymbol{U}_j / \eta_{pj} / \eta_{ej} dt \tag{6}$$

In Equation (6), t_s represents the station-keeping time of the SP.

To facilitate analysis, SP motion can be decomposed into motion along the axis direction and motion along the normal direction. The propeller is assumed to be able to generate thrusts along the axis direction and along the normal direction independently, as illustrated in Figure 1.

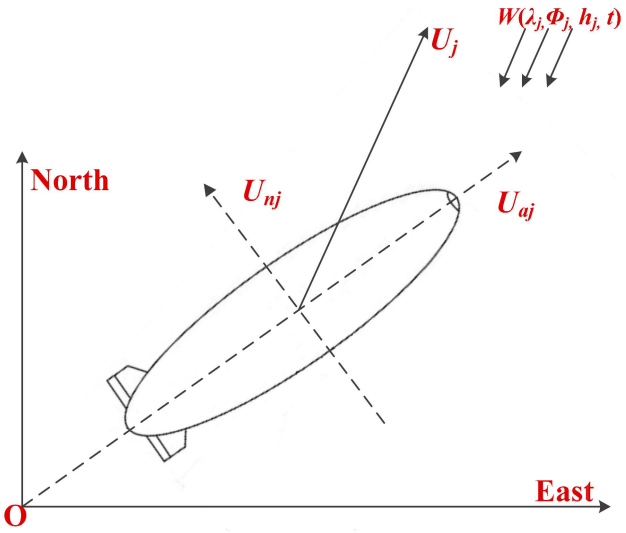

Figure 1. Illustration of an SP motion decomposition in the horizontal plane (since both pitch angle and roll angle of SPs are assumed as 0, this figure only illustrates the motion decomposition in the horizontal plane).

Then, Equation (6) can be rewritten into Equation (7) [23].

$$J_{ej} = \int_0^{t_s} (\boldsymbol{T_{aj}}\boldsymbol{U_{aj}} + \boldsymbol{T_{nj}}\boldsymbol{U_{nj}})/\eta_{pj}/\eta_{ej}dt \tag{7}$$

In Equation (7):
$\boldsymbol{T}_{aj}$ represents the axial component of thrust $\boldsymbol{T}_j$;
$\boldsymbol{U}_{aj}$ represents the axial component of airspeed $\boldsymbol{U}_j$;
$\boldsymbol{T}_{nj}$ represents the normal component of thrust $\boldsymbol{T}_j$;
$\boldsymbol{U}_{nj}$ represents the normal component of airspeed $\boldsymbol{U}_j$;
$\boldsymbol{T}_{aj}$ and $\boldsymbol{T}_{nj}$ can be estimated by aerodynamic resistance, and $\boldsymbol{U}_{aj}$ and $\boldsymbol{U}_{nj}$ can be estimated by local wind speed, as described in Equation (8).

$$\begin{cases} \boldsymbol{T_{aj}} = -\boldsymbol{D_{aj}} = -\frac{1}{2}\rho_{mj}V_j^{2/3}\boldsymbol{U_{aj}^2}C_{Dj} \\ \boldsymbol{U_{aj}} = -\boldsymbol{W}(\lambda_j, \phi_j, h_j, t)\cos(\gamma_j - \gamma_w) \\ \boldsymbol{T_{nj}} = -\boldsymbol{D_{nj}} = -\frac{1}{2}\rho_{mj}V_j^{2/3}\boldsymbol{U_{nj}^2}C_{Dj} \\ \boldsymbol{U_{nj}} = -\boldsymbol{W}(\lambda_j, \phi_j, h_j, t)\sin(\gamma_j - \gamma_w) \end{cases} \tag{8}$$

In Equation (8):
$\boldsymbol{D}_{aj}$ represents the aerodynamic resistance along the axis direction;
$\boldsymbol{D}_{nj}$ represents the aerodynamic resistance along the normal direction;
$\boldsymbol{W}(\lambda_j, \Phi_j, h_j, t)$ represents the wind speed at position (λ_j, Φ_j, h_j) and at time t;
ρ_{mj} represents the atmosphere density at altitude h_j;
V_j represents the volume of the j-th SP, and $V_j^{2/3}$ is used to estimate its reference area;
C_{Dj} represents its aerodynamic resistance coefficient;
γ_w represents the local wind direction angle.
Wind speed $\boldsymbol{W}(\lambda_j, \Phi_j, h_j, t)$, wind direction angle γ_w, and atmosphere density ρ_{mj} change enormously with position, as illustrated in Figures 2–4.

Figure 2 illustrates the meridional and zonal wind speeds in a specific area at an altitude of 20 km. It can be seen from Figure 2 that both meridional wind speed and zonal wind speed vary greatly with latitude in the area. The minimum zonal wind speed is about 8 m/s, while the maximum zonal wind speed has doubled to about 16 m/s. The meridional wind speed has undergone a directional reverse.

Figure 3 illustrates the meridional and zonal wind speeds at a certain location within the altitude interval of 18–30 km at four typical times in March, June, September, and December. From Figure 3, it can be seen that the zonal wind speed varies greatly with altitude changes, whose difference can reach tens of meters. Also, the meridional wind speed shows slight changes.

Figure 4 illustrates the atmospheric density variation of the U.S. standard atmosphere model at an altitude interval of 18–30 km. At an altitude of 18 km, the atmosphere density is about 0.12 kg/m^3, while at an altitude of 30 km, the atmosphere density rapidly decays to less than 0.02 kg/m^3. The attenuation of the atmosphere density exceeds 80%, reflecting a significant change.

These differences illustrated in Figures 2–4 can lead to a huge difference in the energy consumption of a propeller.

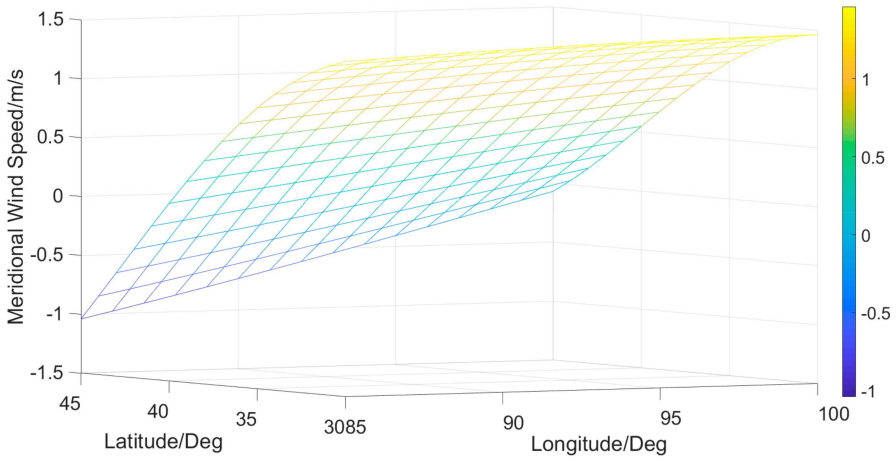

(**a**)

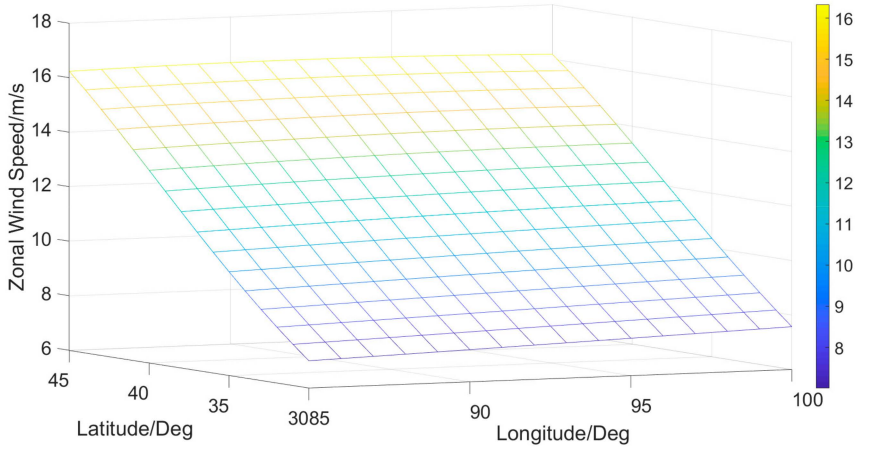

(**b**)

Figure 2. Horizontal wind speeds for a specific region at a certain time: (**a**) meridional wind; (**b**) zonal wind.

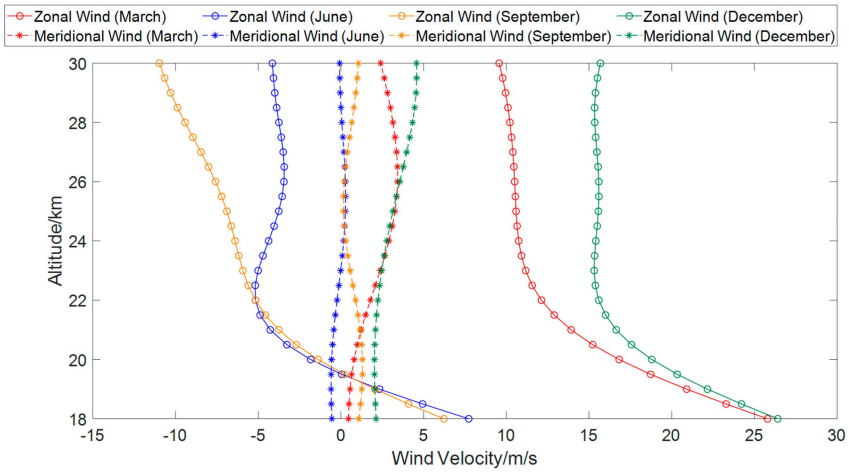

Figure 3. Horizontal winds at different altitudes for a specific region.

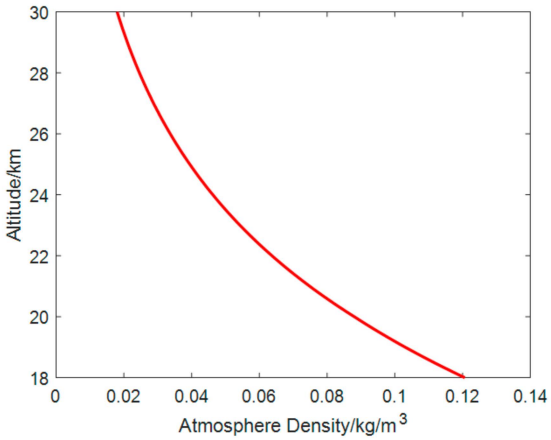

Figure 4. Atmosphere density from 18 km to 30 km according to U.S. Standard Atmosphere, 1976 [24].

3.1.2. Total Energy Consumption of an SP

The energy consumption of other equipment is only slightly affected by the SP position and attitude. Thus, their energy consumption is assumed to be a constant represented by P_{pj}. Their energy consumption, represented by J_{pj}, can be expressed simply by Equation (9).

$$J_{pj} = P_{pj}\, t_s \tag{9}$$

The total energy consumption of the j-th SP, represented by J_j, can be seen as the sum of propeller energy consumption and other equipment energy consumption, which can be expressed by Equation (10).

$$J_j = J_{ej} + J_{pj} \tag{10}$$

3.2. Energy Production of an SP

SP energy production relies on the solar arrays laying on its airship surface, which can convert solar radiation into electricity. Solar radiation harvested by the solar arrays can be divided into direct radiation, scattered radiation, and reflected radiation. Since the effect of scattered radiation and reflected radiation is far less than direct radiation, this paper emphasizes direct radiation and ignores scattered radiation and reflected radiation.

3.2.1. Solar Direct Radiation

The solar direct radiation intensity on the top of the atmosphere in the normal direction, represented by I_{top}, can be expressed by Equation (11) [25].

$$I_{top} = I_{SC}\, E_c \tag{11}$$

In Equation (11), I_{SC} represents the solar constant, and E_c represents a sun–earth distance correction, which can be expressed by Equation (12) [25,26].

$$E_c = 1 + 0.033\cos(2\pi d_n/365) \tag{12}$$

In Equation (12), d_n represents the day number in a year.

The solar direct radiation intensity at different altitudes is affected by the atmosphere transmissivity, which can be expressed by Equation (13) [26].

$$I_{Dj} = I_{top}\tau_j \tag{13}$$

In Equation (13), I_{Dj} and τ_j represent solar direct radiation intensity and atmosphere transmissivity at altitude h_j, respectively. τ_j can be calculated by Equation (14) [27].

$$\tau_j = 0.56(e^{-0.65\lambda mj} + e^{-0.95\lambda mj}) \tag{14}$$

In Equation (14), λ_{mj} can be estimated by Equation (15) [27].

$$\lambda_{mj} = \frac{p_j}{p_0}[\sqrt{1229 + (614\sin\theta_{ej})^2} - 614\sin\theta_{ej}] \tag{15}$$

In Equation (15), p_j represents the pressure of the atmosphere at altitude h_j; p_0 represents the pressure of the atmosphere at sea level.

θ_{ej} represents the solar elevation angle at latitude Φ_j, which can be expressed by Equation (16) [26].

$$\sin\theta_{ej} = \sin\phi_j \sin\delta + \cos\phi_j \cos\delta \cos\omega_j \tag{16}$$

In Equation (16), δ represents sun declination; ω_j represents sun hour angle.

The sun declination δ is the angle of the sun above or below the equator plane. It changes with the date. It will reach its maximum value (23.45 degree) at the summer solstice in the northern hemisphere, and will reach its minimum value (−23.45 degree) at the winter solstice. δ can be roughly calculated by Equation (17) [25].

$$\delta = \begin{cases} 23.45\sin(2\pi(d_n - 81)/365) & d_n > 81 \\ 23.45\sin(2\pi(d_n + 284)/365) & d_n \leq 81 \end{cases} \tag{17}$$

The sun hour angle ω_j is the angle between the sun and the local meridian, which changes 15 degrees per hour and can be calculated by [25].

$$\omega_j = 15(t - 12) \tag{18}$$

3.2.2. Energy Production of a Solar Array

The solar array mounted on the airship surface can be divided into multiple cells to analyze its energy production precisely. If the area of cell k is represented by A_{jk}, the angle of the solar direction vector and the normal vector of cell k is represented by ψ_{jk}, and the output power of cell k produced by solar direct radiation, represented by P_{Djk}, can be calculated by Equation (19) [28,29].

$$P_{Djk} = I_{Dj} A_{jk} cos\psi_{jk} \tag{19}$$

The aggregate output power of all the cells in the solar array, represented by P_{PVj}, can be calculated by Equation (20).

$$P_{PVj} = \sum_{k=1}^{n_c} P_{Djk} \tag{20}$$

In Equation (20), n_c represents the number of solar array cells. The energy production of the j-th SP in its station-keeping time, represented by Q_j, can be expressed as Equation (21).

$$Q_j = \int_0^{t_s} P_{PVj}\eta_{Vj}dt \tag{21}$$

In Equation (21), η_{Vj} represents the photoelectric conversion efficiency of the solar array.

Figure 5 illustrates diurnal energy productions of an SP at different positions, reflecting energy production gaps caused by SP positions.

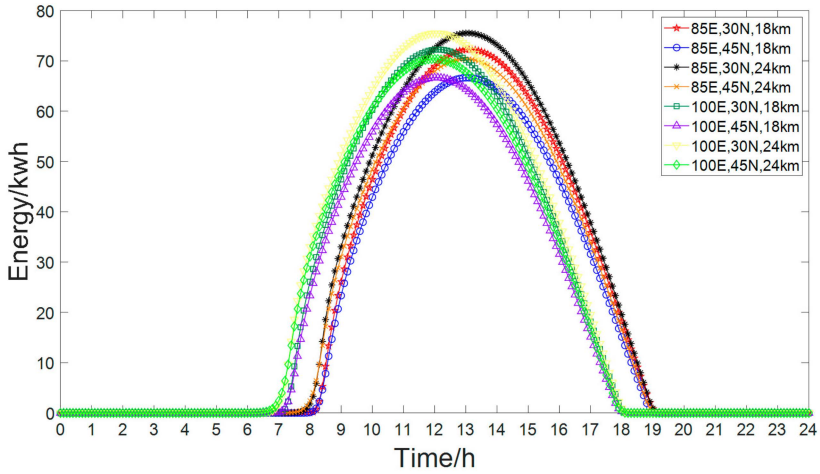

Figure 5. Comparison of energy productions of an SP at different positions on a specific day.

3.3. Energy Balance Indicator of an SPN

According to the analysis above, this paper proposes an energy balance indicator to assess an SP's energy status, which can be formulized as Equation (22).

$$B_j = J_j / Q_j \tag{22}$$

In Equation (22):

J_j represents the energy consumption of the j-th SP, which is defined in Equation (10);

Q_j represents the energy production of the j-th SP, which is defined in Equation (21);

B_j represents the ratio of energy consumption and energy production, reflecting the energy status of the j-th SP.

For an SPN, its energy balance can be assessed by the sum of all the individual energy balance indicators, which can be expressed as Equation (23).

$$B = \sum_{j=1}^{n_p} B_j \tag{23}$$

4. SPN Geometry Optimization Algorithm

4.1. Objective Function and Constraints

SPN design is a multi-objective optimization problem with multiple constraints. This study has two objectives: the first is to minimize SPN GDOP in a given area, which is defined in Equation (1); the second is to minimize the SPN energy balance indicator, which is defined in Equation (23).

Thus, the overall optimization objective function, represented by F, can be expressed as

$$\begin{gathered} F = w_1 GDOP_N + w_2 B \\ w_1 + w_2 = 1 \end{gathered} \tag{24}$$

In Equation (24), w_1 and w_2 represent the weight of GDOP and energy balance in the overall objective function, respectively. Their values can be adjusted within the interval [0, 1] according to requirements, keeping their sum as 1. If w_1 is set as 0, it means that GDOP will be ignored in the process of SPN geometry optimization, and if w_2 is set as 0, it means that energy balance will be ignored.

Two optimization constraints are emphasized in this study. The first is no co-location constraint, meaning that all the SPs in the network should not be deployed in the same position. It can be attributed to the large volume of airships, whose length can reach hundreds of meters. So, a distance is required between SPs to ensure safety, and the distance can be determined according to practical factors such as SP length. The second is

the individual energy balance constraint, requiring each SP in the network to maintain its individual energy balance, which means that for any $j \in [1, n_p]$,

$$B_j < 1 \tag{25}$$

4.2. SPN Geometry Optimization Based on GWO

GWO is a widely used optimization algorithm in many fields [30,31]. It is a meta-heuristic optimization algorithm developed by Mirjalili in 2014 that mimics the hunting behavior and leadership hierarchy of gray wolves [30]. Compared with traditional empirical methods, GWO requires neither gradient information nor continuous derivative of objective functions. Compared with other meta-heuristic optimization algorithms, such as GA, PSO, and SA, GWO has fairly competitive performances [30]. Therefore, GWO is employed in this paper to implement SPN geometry optimization.

In GWO, a solution for a problem is regarded as a gray wolf, and all the available solutions are regarded as a wolf population. Gray wolves in the population are divided into four types: alpha, beta, delta, and omega, representing the current best, sub-optimal, the third best, and other solutions, respectively. The search for the optimal solution is performed by three important strategies: approaching, surrounding, and attacking prey. For a detailed discussion about the strategies, please refer to [30].

In this paper, a gray wolf is defined as the positions of all the SPs in an SPN. The fitness of a gray wolf can be calculated by Equation (24), which represents the weighted sum of GDOP and energy balance indicators, reflecting the comprehensive performance of a gray wolf. From the analysis above, it can be seen that the goal of SPN geometry optimization is to find the SP positions that entail minimizing the objective function (24). This is equivalent to finding the gray wolf that obtains the minimum fitness. Specific steps of SPN geometry optimization can be described as follows [30].

Step 1: Initialize GWO parameters, including population size n_w, maximum iteration number n_m, and others. Set the optimal population fitness as infinite and set the iteration counter as 1.

Step 2: Initialize a gray wolf population randomly.

Step 3: For each gray wolf in the current population, check whether it meets the no co-location constraint discussed in Section 4.1. If not, modify the co-located SP positions until the no co-location constraint is met.

Step 4: For each gray wolf in the current population, check whether it meets the individual energy balance constraint discussed in Section 4.1. If not, set the fitness of the gray wolf as infinite.

Step 5: For each gray wolf to meet the constraints in Section 4.1, calculate its fitness defined in Equation (24).

Step 6: Select the minimal fitness as the optimal population fitness. Update the alpha wolf according to the gray wolf with the minimal fitness.

Step 7: Update all the gray wolves in the population with GWO strategies, such as approaching, surrounding, and attacking prey.

Step 8: For each updated gray wolf, check whether it is outside of the search space. If so, put it on the edge of the search space.

Step 9: Increase the iteration counter by 1.

Step 10: Stop the iteration if the iteration counter reaches the maximum iteration number n_m; otherwise, go to step 3 and continue the iteration.

Step 11: Iteration ends. The current alpha wolf is returned as the optimal solution, and an SPN geometry configuration can be achieved based on the optimal solution.

5. Simulation and Discussion

To verify the proposed algorithm, simulations are carried out in the scenario of SPN positioning. The simulation environment is MATLAB 2018b, and the simulation parameters are shown in Table 2. It is assumed that users are distributed in the service area uniformly with an interval of 0.3 degree, which means there are 11 users in both the longitude direction and the latitude direction.

Table 2. Simulation parameter setting.

Symbolic	Physical Meaning	Value
n_p	number of SPs in the network	6
V_{pj}	volume of stratospheric airship/m^3	100,000
C_{Dj}	aerodynamic resistance coefficient	0.027
η_{ej}	electric motor efficiency	0.7
η_{pj}	propeller propulsive efficiency	0.9
η_{vj}	photoelectric conversion efficiency	16%
P_{pj}	other equipment power/W	100
I_{SC}	the solar constant/W/m^2	1367
n_w	wolf population size	100
n_m	maximum iteration number	50
w_1	weight of GDOP in the objective function	0.5
w_2	weight of energy balance in the objective function	0.5
λ_{min}	minimum longitude/degree	90E
λ_{max}	maximum longitude/degree	93E
Φ_{min}	minimum latitude/degree	37N
Φ_{max}	maximum latitude/degree	40N
h_{min}	minimum altitude to deploy SP/km	18
h_{max}	maximum altitude to deploy SP/km	20
d_{st}	start day of the station-keeping (day number in a year)	80
d_{ed}	end day of the station-keeping (day number in a year)	80
t_{st}	start time of the station-keeping (hour in a day)	0
t_{ed}	end time of the station-keeping (hour in a day)	24
n_u	the number of observers distributed in the service area	121

5.1. Comparison of Simulations with/without Consideration of Energy Balance Requirement

To compare the proposed algorithm and traditional algorithms without consideration of the energy balance requirement, two simulations are carried out with almost the same steps and conditions as listed above, except for two differences.

The first difference is the weight assignment in the optimization object function, i.e., w_1 and w_2 in Equation (24). In the simulation without considering the energy balance requirement, w_1 is set as 1 and w_2 is set as 0. In the simulation with consideration of the energy balance requirement, both w_1 and w_2 are set as 0.5.

The second difference is the individual energy balance constraint. In the simulation without consideration of the energy balance requirement, the constraint is ignored, i.e., step 3 of the optimization procedure in Section 4.2 is omitted. In the simulation with consideration of the energy balance requirement, step 3 is executed.

The simulation results are listed in Table 3 and Figures 6 and 7.

In Table 3 and subsequent simulation result tables, columns λ_j, Φ_j, and h_j list the longitudes, latitudes, and altitudes of all the SPs in the SPN, column B_j lists the values of the energy balance indicators for all the SPs in the SPN, column B lists the value of the energy balance indicator for the SPN, column $GDOP_N$ lists the GDOP value for the SPN, and column F lists the fitness of the SPN. For columns B_j, B, $GDOP_N$, and F in these tables, the smaller their value is, the better the SPN geometry performance is.

Table 3. Comparison of simulations with/without consideration of energy balance requirement.

	λ_j/deg, Φ_j/deg, h_j/km	Bj	B	$GDOP_N$	F
with consideration of energy balance requirement	92.7E, 37.0N, 19.5	0.35	1.75	7.52	4.64
	92.4E, 39.4N, 20.0	0.29			
	90.6E, 38.5N, 20.0	0.25			
	92.1E, 37.9N, 20.0	0.23			
	90.0E, 39.7N, 20.0	0.29			
	90.6E, 37.0N, 19.5	0.34			
without consideration of energy balance requirement	91.8E, 38.8N, 18.5	1.11	5.88	7.36	7.36
	90.3E, 39.4N, 18.5	1.12			
	90.3E, 37.6E, 18.5	1.03			
	91.5E, 37.9N, 19.0	0.64			
	93.0E, 37.0N, 18.0	1.67			
	93.0E, 40.0N, 20.0	0.31			

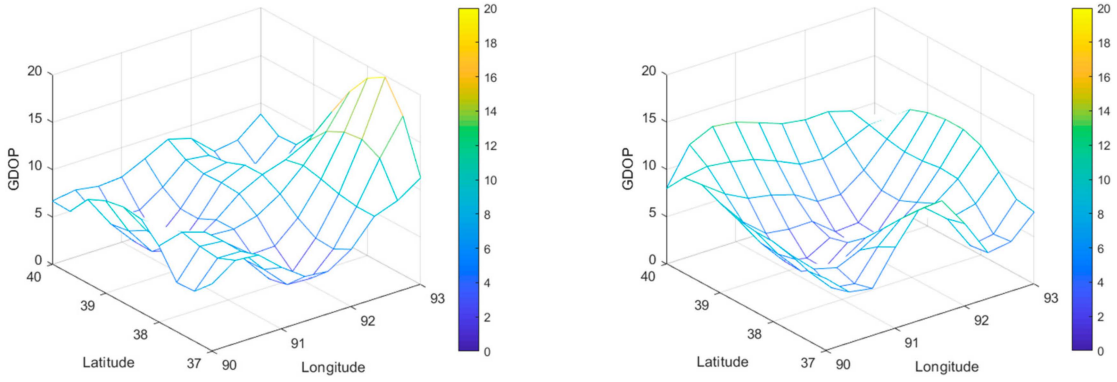

(**a**) (**b**)

Figure 6. GDOP distribution of SPNs: (**a**) SPN with consideration of energy balance requirement; (**b**) SPN without consideration of energy balance requirement.

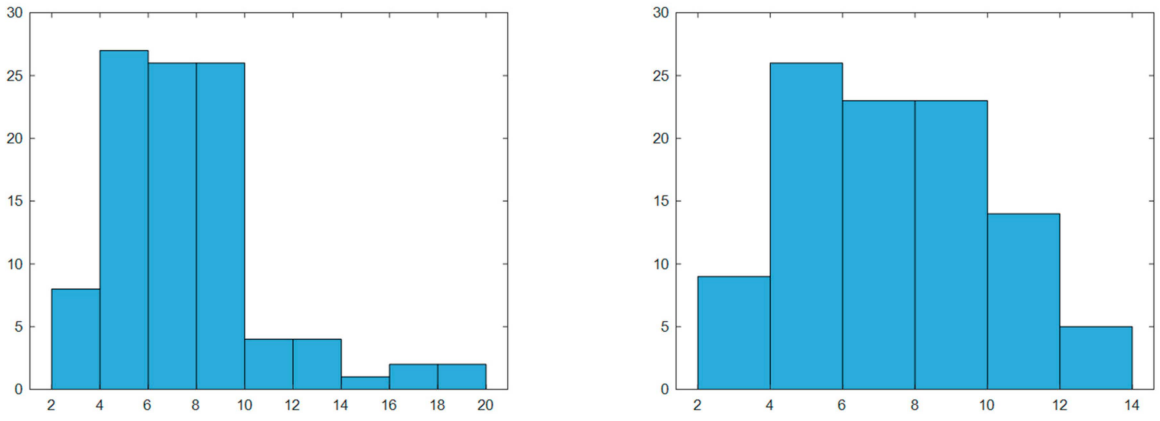

(**a**) (**b**)

Figure 7. GDOP histogram of SPNs: (**a**) SPN with consideration of energy balance requirement; (**b**) SPN without consideration of energy balance requirement.

Column B_j in Table 3 implies that geometry configuration has a significant impact on SPN energy balance. For the same SP, their energy balance indicator can differ by several times at different locations.

Column *B* in Table 3 also proves the necessity of energy balance analysis in SPN geometry design. If it is ignored, an SPN with unacceptable energy performance might be obtained, as shown in the 7th, 8th, 9th, and 11th row of Table 3 (B_j = 1.11, 1.12, 1.03, and 1.67, respectively). The station-keeping capacity of such an SPN is very poor, which will degrade the SPN availability and continuity.

In contrast, by assigning a weight to the energy balance indicator properly in the objective function and implementing an individual energy balance constraint, the proposed algorithm can avoid unacceptable results effectively. Furthermore, in terms of GDOP, the results of the algorithm considering energy are not much worse than those of algorithms that do not consider energy.

5.2. Comparison among Different Altitude Intervals

In this section, the values of h_{min} and h_{max} in Table 2 are adjusted to compare SPN geometry performances at different altitudes. Simulations in this section and subsequent sections are implemented with consideration of the energy balance requirement.

Simulation results are shown in Table 4 and Figures 8 and 9.

Table 4. Comparison of SPNs in different altitude intervals.

Altitude Interval/km	λ_j/deg, Φ_j/deg, h_j/km	*Bj*	*B*	$GDOP_N$	*F*
18~20	92.7E, 37.0N, 19.5	0.35	1.75	7.52	4.64
	92.4E, 39.4N, 20.0	0.29			
	90.6E, 38.5N, 20.0	0.25			
	92.1E, 37.9N, 20.0	0.23			
	90.0E, 39.7N, 20.0	0.29			
	90.6E, 37.0N, 19.5	0.34			
20~22	90.9E, 38.5N, 21.0	0.10	0.52	7.12	3.82
	90.0E, 40.0N, 21.5	0.10			
	90.6E, 37.0N, 21.5	0.05			
	92.4E, 39.1N, 22.0	0.06			
	92.1E, 37.6N, 20.5	0.13			
	93.0E, 37.6N, 21.0	0.08			
22~24	92.4E, 37.9N, 22.0	0.04	0.23	6.29	3.26
	93.0E, 40.0N, 24.0	0.03			
	91.8E, 39.1N, 22.0	0.06			
	91.2E, 39.7N, 23.0	0.04			
	90.0E, 37.0N, 22.0	0.03			
	90.9E, 37.9N, 23.0	0.03			
24~26	90.9E, 38.2N, 26.0	0.01	0.11	5.58	2.84
	93.0E, 40.0N, 26.0	0.02			
	92.1E, 37.6N, 25.0	0.01			
	90.0E, 39.7N, 25.0	0.03			
	90.0E, 37.0N, 24.0	0.02			
	92.1E, 39.1N, 25.5	0.02			
26~28	93.0E, 40.0N, 28.0	0.01	0.06	5.35	2.71
	90.6E, 39.7N, 27.5	0.01			
	92.4E, 37.6N, 26.5	0.01			
	90.0E, 37.0N, 26.0	0.01			
	92.1E, 39.1N, 28.0	0.01			
	90.6E, 37.9N, 27.5	0.01			

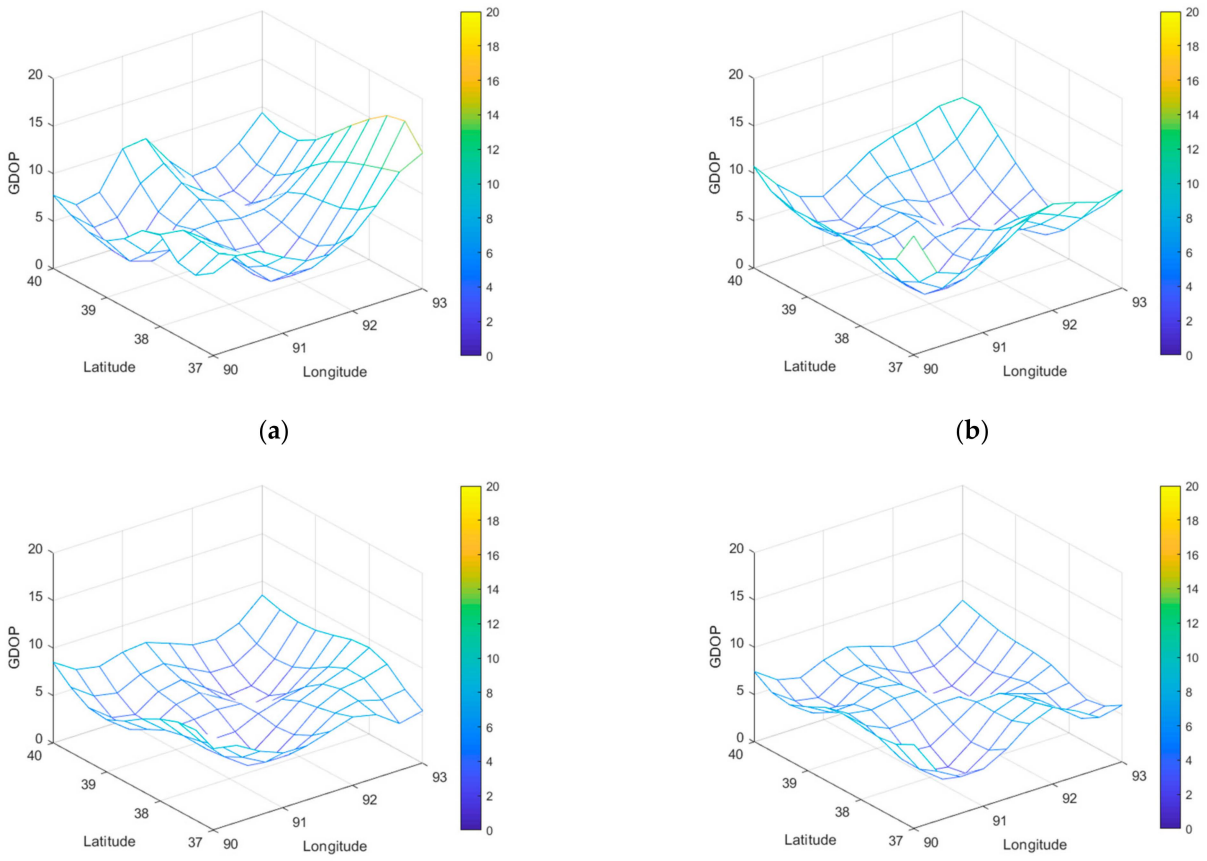

Figure 8. GDOP distribution of SPNs in different altitude intervals: (**a**) SPNs in 20~22 km; (**b**) SPNs in 22~24 km; (**c**) SPNs in 24~26 km; (**d**) SPNs in 26~28 km (for GDOP distribution of SPNs in 18~20 km, please refer to Figure 6a).

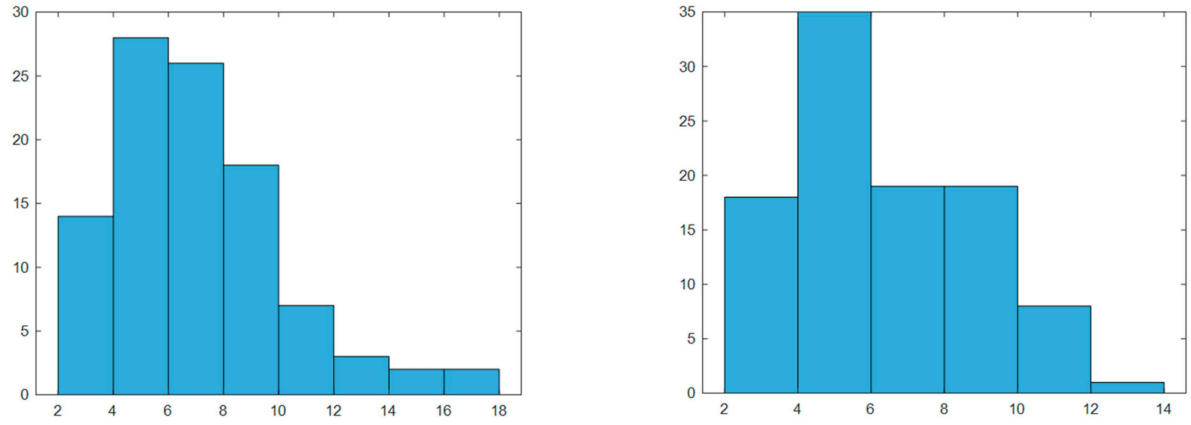

Figure 9. *Cont.*

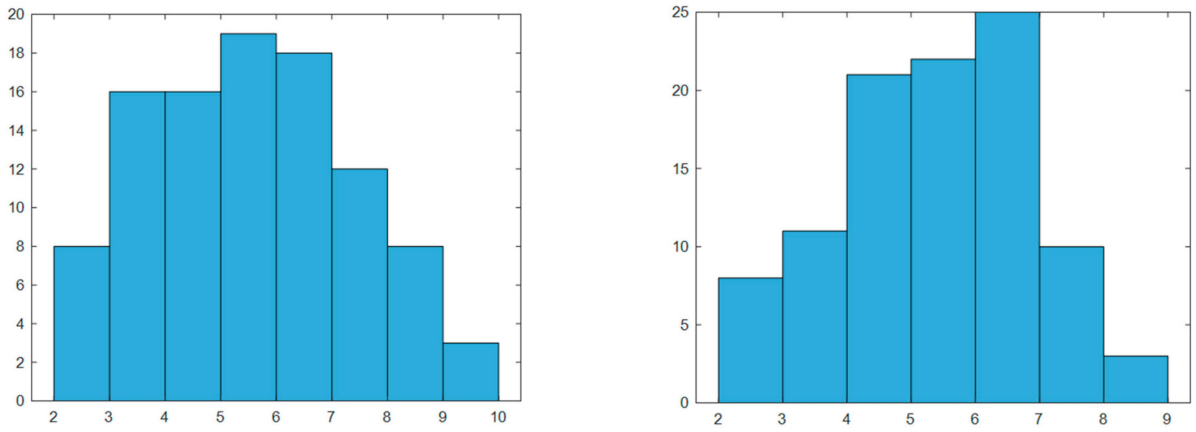

(**c**) (**d**)

Figure 9. GDOP histogram of SPNs in different altitude intervals: (**a**) SPNs in 20~22 km; (**b**) SPNs in 22~24 km; (**c**) SPNs in 24~26 km; (**d**) SPNs in 26~28 km (for GDOP histogram of SPNs in 18~20 km, please refer to Figure 7a).

The results in Table 4 and Figures 8 and 9 imply that under the given conditions, both GDOP and the energy balance indicator show a decreasing trend with the altitude increasing from 18 km to 28 km, meaning that SPN geometry performance improves as altitude increases in this altitude interval.

The decrease in the energy balance indicator can be attributed to wind, atmosphere, solar radiation, and other factors.

From Figure 3, it can be seen that in March, as the altitude increases from 18 km to 28 km, the zonal wind speed decreases from over 20 m/s to less than 10 m/s, while the increase in the meridional wind speed is less than 5 m/s, resulting in a decrease in energy consumption for the SP. From Figure 4, it can be seen that as the altitude increases, the atmosphere density decreases, which is also beneficial for reducing energy consumption.

From Figure 10, it can be seen that the atmosphere pressure decreases as the altitude increases. From Equations (13)–(15), it can be inferred that solar direct radiation intensity increases as the altitude increases, which can lead to an increase in SP energy production, as illustrated in Figure 5.

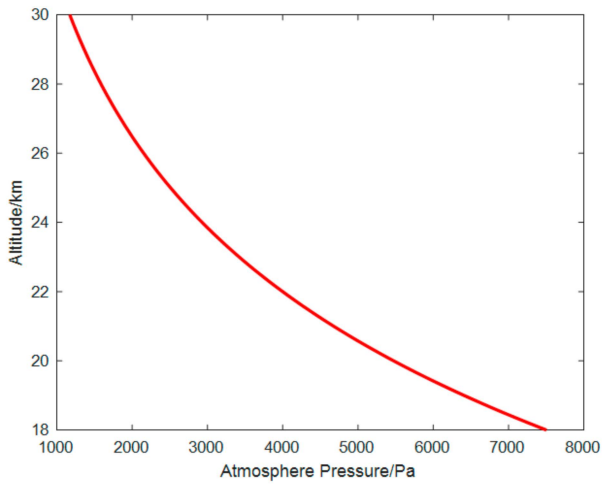

Figure 10. Atmosphere pressure from 18 km to 30 km according to U.S. Standard Atmosphere, 1976 [24].

Therefore, the energy balance indicator, which is the ratio of energy consumption and energy production, decreases as the altitude increases.

In addition, as the altitude increases, the value of the SPN elevation angle increases, which can improve the GDOP of the SPN. This has been deduced and explained in detail in [8,10].

Therefore, both the energy balance indicator and GDOP will improve as the altitude increases, as shown in Table 4, Figure 8, and Figure 9. So, an SPN with a higher station-keeping altitude is expected in order to achieve a better performance under the given conditions.

5.3. Comparison among Different Latitude Intervals

In this section, the values of Φ_{min} and Φ_{max} in Table 2 are adjusted to compare network performances in different latitudes. Simulation results are shown in Table 5.

Table 5. Comparison among SPNs of different latitude intervals.

Latitude Interval/deg	λ_j/deg, Φ_j/deg, h_j/km	Bj	B	$GDOP_N$	F
33~36N	91.5E, 35.1N, 20.0 92.4E, 33.0N, 19.5 93.0E, 36.0N, 20.0 90.0E, 34.2N, 20.0 90.0E, 36.0N, 19.0 91.8E, 33.9N, 20.0	0.15 0.20 0.17 0.12 0.54 0.12	1.30	7.15	4.23
35~38N	90.6E, 35.3N, 19.5 92.4E, 35.3N, 19.0 92.1E, 36.8N, 20.0 93.0E, 38.0N, 20.0 91.2E, 36.2N, 20.0 91.2E, 37.7N, 20.0	0.28 0.52 0.19 0.23 0.17 0.22	1.61	7.32	4.47
37~40N	92.7E, 37.0N, 19.5 92.4E, 39.4N, 20.0 90.6E, 38.5N, 20.0 92.1E, 37.9N, 20.0 90.0E, 39.7N, 20.0 90.6E, 37.0N, 19.5	0.35 0.29 0.25 0.23 0.29 0.34	1.75	7.52	4.64
39~42N	92.1E, 41.4N, 19.5 90.9E, 39.0N, 20.0 93.0E, 42.0N, 20.0 90.9E, 39.9N, 19.5 92.1E, 40.2N, 20.0 90.3E, 41.4N, 19.5	0.55 0.27 0.40 0.47 0.32 0.54	2.55	7.12	4.83
41~44N	90.9E, 41.9N, 20.0 93.0E, 44.0N, 20.0 90.0E, 41.0N, 20.0 90.3E, 42.8N, 20.0 91.8E, 43.1N, 19.5 92.4E, 42.2N, 19.0	0.39 0.49 0.35 0.43 0.63 0.85	3.14	6.89	5.02

The results detailed in Table 5 imply that low latitude intervals tend to be beneficial to the network energy balance while having little impact on SPN GDOP under the given conditions.

From Figure 2, it can be seen that within the service area listed in Table 5, as the latitude decreases, the zonal wind speed decreases significantly, which can reduce SP energy consumption. From Figure 5, it can be seen that lower latitude can help SPs obtain more energy production. Therefore, the SPN energy balance indicator shows a decreasing tendency with decreasing latitude.

6. Conclusions and Future Works

SPN is a novel aerial network with promising potential. Geometry design is a critical problem affecting its service performance significantly. This paper focuses on SPN geometry design to pursue a satisfactory performance for both GDOP and energy balance. In the assumed service area and under the given simulation conditions, the following conclusions can be drawn:

Geometry configuration has a significant impact on both SPN energy balance and GDOP. Consequently, neither of them can be ignored in SPN geometry design.

The energy balance requirement of an SPN can be met by properly assigning weights on the energy balance indicator in the objective function and implementing the energy balance constraint of individual SPs.

Both GDOP and energy balance can be improved by raising the station-keeping altitude towards the altitude interval of 26~28 km.

GDOP shows no substantial improvement when the deployment space is slightly adjusted southward and northward. Energy balance tends to improve gently when deployment space moves southward.

Some issues can be analyzed in the future.

In this paper, the photoelectric conversion efficiency of the solar array is assumed to be constant. However, it changes with the thermal conditions in practice. In the future, the influence of photoelectric conversion efficiency fluctuation on SP energy production and energy balance should be analyzed.

Also, uncertain wind is ignored in this paper since the wind at the altitude interval of SP is relatively stable, but uncertain wind exists according to [32], and it may have an impact on the energy consumption of SPs. Further analysis can be conducted next.

In addition, this paper implements simulations currently just for a small area. More simulations for larger areas can be carried out according to requirements.

Author Contributions: Conceptualization, Y.Q.; methodology, Y.Q. and S.W.; software, Y.Q.; validation, H.F. and Q.L.; writing—original draft preparation, Y.Q.; writing—review and editing, S.W. and H.F.; visualization, Y.Q.; supervision, S.W. All authors have read and agreed to the published version of the manuscript.

Funding: This work was funded by the National Key Research and Development Program of China (Grant No. 2022YFB3901805).

Data Availability Statement: Data are contained within the article.

Conflicts of Interest: The authors declare no conflicts of interest.

References

1. Tsujii, T.; Rizos, C.; Wang, J.; Dai, L.; Roberts, C. A navigation/positioning service based on pseudolites installed on stratospheric airships. *Jpn. Soc. Aeronaut. Space Sci.* **2003**, *50*, 36. [CrossRef]
2. Dovis, F.; Presti, L.; Mulassano, P. Support infrastructures based on high altitude platforms for navigation satellite systems. *IEEE Wirel. Commun.* **2005**, *12*, 106–112. [CrossRef]
3. Zheng, H.; Atia, M.; Yanikomeroglu, H. High Altitude Platform Station (HAPS)-Aided GNSS for Urban Areas. *arXiv* **2023**. [CrossRef]
4. Chandu, B.; Pant, R.S.; Moudgalya, K. Modeling and simulation of a precision navigation system using pseudolites mounted on airships. In Proceedings of the 7th AIAA ATIO Conf, 2nd CEIAT Int'l Conf on Innov and Integr in Aero Sciences, 17th LTA Systems Tech Conf, Belfast, UK, 18–20 September 2007. [CrossRef]
5. Dai, L.W.; Wang, J.L.; Tsujii, T.; Rizos, C. Pseudolite applications in positioning and navigation: Modelling and geometric analysis. *J. Navig.* **2004**. Available online: https://www.researchgate.net/profile/Jinling_Wang2/publication/2865922_Pseudolite_applications_in_positioning_and_navigation_Modelling_and/links/546d98510cf26e95bc3cb846.pdf?__cf_chl_tk=NFi8SdAKc5gBoKKe9i2BXt_BS1bZjkE2X5PooWMY56U-1717999627-0.0.1.1-8446 (accessed on 4 June 2024).
6. Fateev, Y.L.; Ratuschnyak, V.N.; Kartson, I.N.; Tyapkin, V.N.; Dmitriev, D.D.; Goncharov, A.E. Analyzing measurement errors for navigation parameters in onground short-range navigation systems based on pseudolites. *IOP Conf.* **2016**, *155*, 012016. [CrossRef]
7. Sang, W.G.; He, X.F.; Chen, Y.Q. Configuration of pseudolite-alone positioning system based on DOP geometry structure. *Bull. Surv. Mapp.* **2013**, *9*, 1–4.
8. Hu, W.; Yang, J.J.; He, P. Study on pseudolite configuration scheme based on near space airships. *Radio Eng.* **2009**, *39*, 24–27.

9. Gao, S.S.; Zhao, F.; Xie, M.L. Research on the geometric configuration scheme of near space pseudolite-only positioning system. *J. Navig. Position.* **2013**, *1*, 21–25.
10. Yang, Y.; Gao, S.S.; Yan, H.F. Design on geometric configuration schemes of pseudolite in near space. *Syst. Eng. Electron.* **2014**, *36*, 532–538.
11. Mosavi, M.R.; Divband, M. Calculation of geometric dilution of precision using adaptive filtering technique based on evolutionary algorithms. In Proceedings of the 2010 International Conference on Electrical and Control Engineering, Wuhan, China, 25–27 June 2010. [CrossRef]
12. Shao, K.; Li, K.; Wang, J. PSO-Based pseudolite layout strategy. *Commun. Technol.* **2017**, *50*, 2454–2459.
13. Tang, W.J.; Chen, J.P.; Yu, C.; Ding, J.; Wang, R. A new ground-based pseudolite system deployment algorithm based on MOPSO. *Sensors* **2021**, *21*, 5364. [CrossRef]
14. Yang, L.; Zhou, J.H.; Chen, J.P. The study of optimization of formation flying navigation augmentation platforms based on genetic algorithm. *GNSS World China* **2008**, *33*, 9–13.
15. Chen, C.; Chen, K.; Huang, J.; Li, Y. Using genetic algorithms to approximate weighted geometric dilution of precision. In Proceedings of the 2016 International Symposium on Computer, Consumer and Control (IS3C), Xi'an, China, 4–6 July 2016. [CrossRef]
16. Song, J.; Hou, C.; Xue, G.; Ma, M. Study of constellation design of pseudolites based on improved adaptive genetic algorithm. *J. Commun.* **2016**, *11*, 879–885. [CrossRef]
17. Araripe, D.F.; De, M.F.; Campos, D.T. High-altitude platforms—Present situation and technology trends. *J. Aerosp. Technol. Manag.* **2016**, *8*, 249–262. [CrossRef]
18. Nickol, C.L.; Guynn, M.D.; Kohout, L.L.; Ozoroski, T.A. High Altitude Long Endurance UAV Analysis of Alternatives and Technology Requirements Development. In Proceedings of the 45th AIAA Aerospace Sciences Meeting and Exhibit, Reno, NV, USA, 8–11 January 2007. [CrossRef]
19. Yang, X.; Wang, F.; Liu, W.; Xiao, W.; Ye, X. A Layout Method of Space-Based Pseudolite System Based on GDOP Geometry. *Chin. J. Electron.* **2023**, *32*, 1050–1058. [CrossRef]
20. Sultana, Q.; Sunehra, D.; Srinivas, V.S.; Sarma, A.D. Effects of Pseudolite Positioning on DOP in LAAS. *Positioning* **2010**, *1*, 18–26. [CrossRef]
21. Jiang, M.; Li, R.; Liu, W. Research on geometric configuration of pseudolite positioning system. *Comput. Eng. Appl.* **2017**, *53*, 271–276.
22. Zhao, Y.; Garrard, W.; Mueller, J. Benefits of Trajectory Optimization in Airship Flights. In Proceedings of the AIAA 3rd "Unmanned Unlimited" Technical Conference, Workshop and Exhibit, Chicago, IL, USA, 20–23 September 2004. [CrossRef]
23. Wu, L.; Li, Y.; Li, Z. The research of route planning for stratospheric airships based on genetic algorithms. *Spacecr. Recovery Remote Sens.* **2011**, *32*, 1–6.
24. *NOAA-S/T-76-1562*; U.S. Standard Atmosphere, 1976. National Oceanic and Atmospheric Administration; National Aeronautics and Space Administration; United States Air Force: Washington, DC, USA, 1976.
25. Stanciu, C.; Stanciu, D. Optimum tilt angle for flat plate collectors all over the World—A declination dependence formula and comparisons of three solar radiation models. *Energy Convers. Manag.* **2014**, *81*, 133–143. [CrossRef]
26. Zhang, L.; Li, J.; Jiang, Y.; Du, H.; Zhu, W.; Lv, M. Stratospheric airship endurance strategy analysis based on energy optimization. *Aerosp. Sci. Technol.* **2020**, *100*, 105794. [CrossRef]
27. Long, Y.; Deng, X.; Yang, X.; Hou, Z. Trajectory simulation of stratosphere aerostats in polar vortex wind field. *Comput. Simul.* **2021**, *38*, 37–42.
28. Lv, M.; Li, J.; Du, H.; Zhu, W.; Meng, J. Solar array layout optimization for stratospheric airships using numerical method. *Energy Convers. Manag.* **2017**, *135*, 160–169. [CrossRef]
29. Zhang, Y.; Li, J.; Lv, M.; Tan, D.; Zhu, W.; Sun, K. Simplified analytical model for investigating the output power of solar array on stratospheric airship. *Int. J. Aeronaut. Space Sci.* **2016**, *17*, 432–441. [CrossRef]
30. Mirjalili, S.; Mirjalili, S.M.; Lewis, A. Grey wolf optimizer. *Adv. Eng. Softw.* **2014**, *69*, 46–61. [CrossRef]
31. Arora, S.; Singh, H.; Sharma, M.; Sharma, A.; Anand, P. A new hybrid algorithm based on grey wolf optimization and crow search algorithm for unconstrained function optimization and feature selection. *IEEE Access* **2019**, *7*, 26343–26361. [CrossRef]
32. Conway, J.P.; Bodeker, G.E.; Waugh, D.W.; Murphy, D.J.; Cameron, C.; Lewis, J. Using project Loon superpressure balloon observations to investigate the inertial peak in the intrinsic wind spectrum in the midlattitude stratosphere. *J. Geophys. Res. Atmos.* **2019**, *124*, 8594–8604. [CrossRef]